EURASIAN PHYSICAL TECHNICAL JOURNAL

2026, Volume 23, No. 1 (55)

https://doi.org/10.31489/2026N1/130-137

Received: 13/10/2025 Revised: 29/01/2026 Accepted: 19/03/2026 Published online:30/03/2026

Original Research Article

UDC 53.087; 524.3-52

IDENTIFICATION OF COMPLEX ORGANIC MOLECULES IN THE HOT MOLECULAR CORE G335.79+0.17

Abdirakhman A.A.[1], OmarA.Zh. [1,*], Alimgazinova N.Sh.[1], Tuiakbayeva D.R.[2], Baitursyn D.Y.[3]

[1] Al-Farabi Kazakh National University, Almaty, Kazakhstan
[2] Sh. Ualikhanov Kokshetau University, Kokshetau, Kazakhstan
[3] Astana Motors Manufacturing Kazakhstan, Almaty, Kazakhstan

Corresponding author: omaruzhan@gmail.com

Abstract. *Observations of the massive star-forming region G335.79+0.17 reveal dense, hot molecular gas toward two cores, P1 and P2, traced by methyl cyanide, its isotopologue, methyl acetylene, formaldehyde and dust continuum emission. Only these two hot cores are detected, highlighting a chemically rich environment typical of early massive star formation. Velocity gradients in opposite directions provide strong evidence of molecular gas rotation. Rotational diagram analysis shows that core P1 is hotter than P2, with methyl cyanide and its isotopologue tracing gas near the protostar, while methyl acetylene traces cooler outer layers.*

Keywords: star formation, massive stars, hot molecular core, individual object G335.79+0.17.

1. Introduction

High-mass star-forming regions (HMSFRs) are among the most dynamic and chemically rich environments in the interstellar medium (ISM), hosting the earliest stages of massive star formation. High-mass stars ($M > 8\ M_{\odot}$) form within massive ($\sim 10^3\ M_{\odot}$) and dense (10^4–$10^5\ cm^{-3}$) molecular clumps, typically ~1 pc in size and supported by turbulent motions [1-3]. These clumps harbor luminous, embedded infrared sources known as high-mass young stellar objects (HMYSOs), which represent the early evolutionary stages of individual massive stars or multiple stellar systems. Massive star formation frequently takes place in highly dynamic environments where large-scale processes such as cloud–cloud collisions and filamentary accretion play a central role in gas compression and clustered star formation [4,5]. These mechanisms not only enhance star formation efficiency but can also trigger core–core interactions within dense molecular clumps, further driving the growth of massive protostars [6,7]. Alternatively, similar morphologies may result from hub–filament systems, where gravitational collapse and ordered accretion flows feed dense cores [8-11]. In addition to collisional and filamentary accretion scenarios, stellar feedback from evolved systems can both trigger and suppress star formation [12-14].

Star-forming regions are also key environments for the build-up of chemical complexity in the ISM. The molecules found in these regions trace chemical processes that give rise to complex species. Complex organic molecules (COMs) are generally defined as carbon-bearing species with six or more atoms [15]. Their formation routes, whether in the gas phase or on dust grains, remain uncertain. Symmetric top molecules serve as valuable tracers of gas temperature, with methyl acetylene (CH_3CCH) and methyl cyanide (CH_3CN) being

prominent examples [16]. Formaldehyde (H_2CO), a key precursor of CH_3OH in grain-surface chemistry, is a well-established tracer of gas kinetic temperature owing to its slightly asymmetric rotor structure [17,18]. H_2CO has been widely used to probe dense gas in both nearby molecular clouds [19,20] and massive complexes such as Cygnus-X [21]. G335.79+0.17 has been identified as a Class II methanol maser and an OH maser source [22], and is thought to be located at a distance of 3.4 kpc [23]. Its mid-infrared Spitzer properties are consistent with a high-mass young stellar object (HMYSO) [24]. Studying dynamic and chemically rich regions can be guided by methods used in other rapidly evolving astrophysical systems, where early, multi-band observations have been crucial for determining their physical and chemical properties [25].

The main aim of this work is to investigate the emission properties of CH_3CCH, CH_3CN and H_2CO toward the hot molecular core in G335.79+0.17. The analysis aims to constrain the physical and chemical structure of the core by deriving gas temperature, column density and kinematic properties, thereby clarifying the evolutionary stage of the embedded HMYSO.

2. Observations and data reduction

Archival ALMA Band 7 data (Project 2021.1.00720.S) covering the frequency range 275.596–291.491 GHz were used to investigate molecular line emission toward the G335.79+0.17 region. The observations were carried out in April 2022 with the 12 m array. The array configuration provided baseline lengths between 25.201 m and 183.800 m, yielding a synthesized beam size of 0. ″670.

The spectral setup consisted of seven spectral windows, spanning the ranges 275.612–278.080 GHz, 277.113–278.987 GHz, 289.964–290.433 GHz, 290.447–290.564 GHz, 290.615–290.732 GHz, 291.227–291.344 GHz, and 291.370–291.487 GHz. The phase center was set at $\alpha(J2000) = 16^h29^m47^s$, $\delta(J2000) = -48°15'52''$, and the resulting data cube has a spectral resolution of 282.227 kHz. The systemic velocity of the source is approximately -50 km s^{-1}. Calibration and reduction were performed using the Common Astronomy Software Applications package (CASA) [26]. The continuum emission was subtracted in the visibility domain using the CASA task uvcontsub, which fits and removes continuum emission from line-free channels. The resulting continuum-subtracted visibilities were then imaged using the CASA task tclean to produce spectral line data cubes and continuum images.

3. Results and discussion

The dust continuum emission traces the distribution of dense material and enables the identification of compact cores that host ongoing star formation. In contrast, the H_2CO emission delineates filamentary and streamer-like dense gas surrounding the hot cores, thereby providing complementary information to the continuum morphology. The H_2CO ($4_{2,3}$–$3_{2,2}$) transition at 291.238 GHz was analyzed together with ALMA 1.1 mm continuum data to investigate G335.79+0.17. Figure 1 shows the H_2CO ($4_{2,3}$-$3_{2,2}$) moment 0 map with overlaid 1.1 mm dust continuum contours, along with several maser spots indicated: H_2CO at 22 GHz (white triangle), OH at 1665 MHz (yellow triangle), CH_3OH Class II at 38.2 GHz (blue triangle), and CH_3OH at 6.67 GHz (black triangle). The H_2CO moment 0 emission is concentrated in two peaks, corresponding to the continuum, which are associated with the hot cores G335.78+0.17 P1 and P2. These cores were previously reported with systemic velocities of -51 km s^{-1} and -46 km s^{-1} at a distance of 3.4 kpc. For consistency, the same nomenclature is adopted, referring to them as cores P1 and P2. At this distance, their projected separation of 12.25″ corresponds to ≈0.2 pc. Core P1 exhibits a U-shaped morphology elongated along the east–west direction, with an integrated H_2CO intensity of 4 Jy $beam^{-1}$ km s^{-1}, brighter than that of P2 (3 Jy $beam^{-1}$ km s^{-1}). Their physical parameters, derived from 2D Gaussian fitting of the continuum emission with CARTA, are summarized in Table 1.

Table 1. Derived parameters of the continuum sources in G335.79+0.17.

Source	RA (J2000)	DEC (J2000)	FWHM (″) Major × Minor	Peak (Jy $beam^{-1}$)	Flux (Jy)
P1	$16^h29^m47^s51 \pm 0.0002$	−48°15′48″05 ± 0.01″	2.21 ± 0.02 × 0.99 ± 0.01	3.54 ± 0.03	18.09 ± 0.20
P2	$16^h29^m47^s13 \pm 0.002$	−48°15′50″02 ± 0.02″	0.70 ± 0.04 × 1.16 ± 0.08	0.10 ± 0.01	0.19 ± 0.02

Figure 2 presents the molecular line spectra toward G335.79+0.17 P1, extracted from a circular region with a diameter of 0.9″ centered at (RA, Dec) = (16:29:47.3388, −48°15′52.3963″). The upper panel shows

nine K-components (K = 0–8) of the CH_3CN J = 15 → 14 transition (blue) and seven K-components (K = 0–6) of the $CH_3{}^{13}CN$ J = 15 → 14 transition (red), along with CH_3OH v_t = 0, 26(3,24)-26(2,25)$^{+-}$ at 275.663 GHz; CH_3OCHO: v = 1, 23(4,20)-22(4,19) A at 275.766 GHz, 46(11,36)-45(12,33) E at 275.698 GHz; $(CH_3)_2CO$ 14(13,2)-13(12,2) EE at 275.741 GHz. The lower panel displays the CH_3CCH J = 17 → 16 transition, detected over 290.413–290.502 GHz with five K-components (K = 0–4).

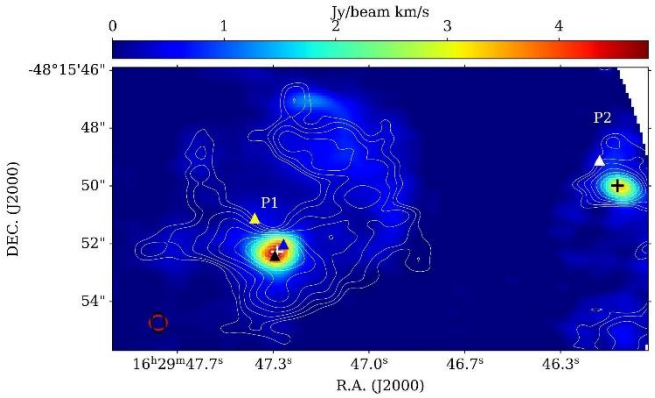

Fig.1. Moment 0 color map of the H_2CO ($4_{2,3}$-$3_{2,2}$) emission, overlaid with contours of the 1.1 mm dust continuum emission toward G335.79+0.17. Contours are plotted at 1σ, 5σ, 20σ, 100σ, and 600σ, where σ = 0.005 Jy beam^{-1}. The synthesized beam of the continuum (red) and H_2CO (black) is shown in the lower left corner.

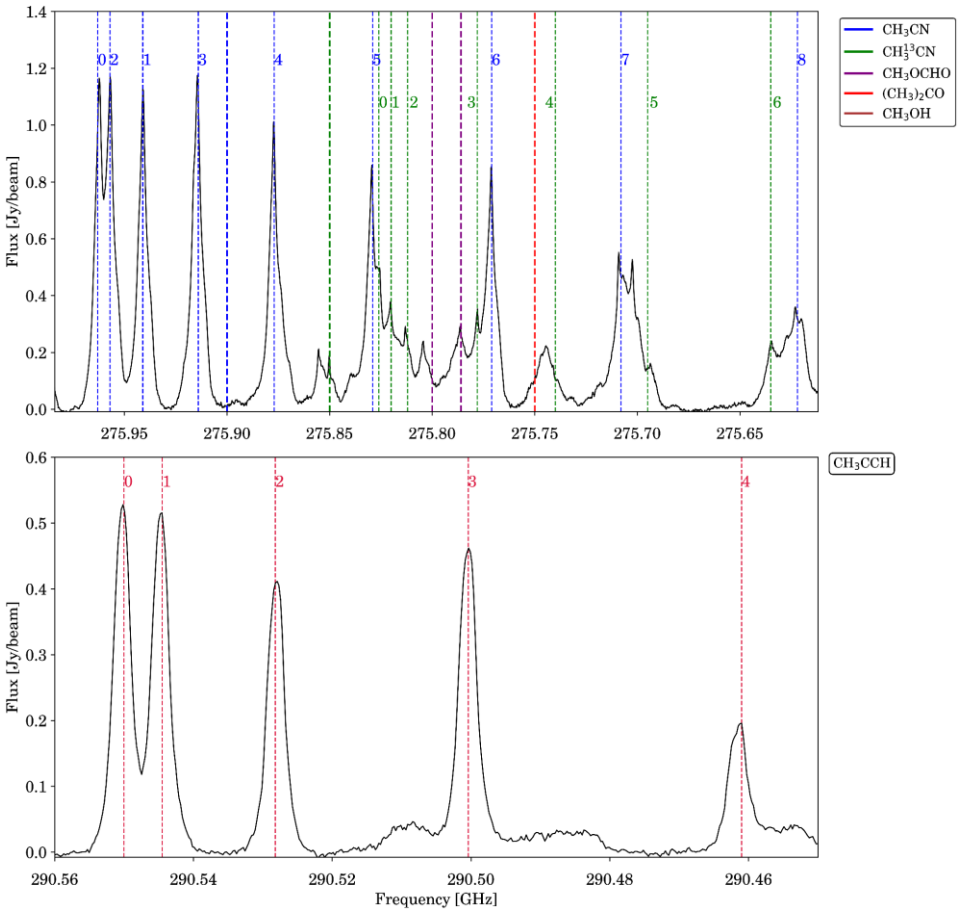

Fig. 2. Molecular line spectra toward G335.79+0.17 P1, extracted from a circular region with a diameter of 0.9″ centered at (RA, Dec) = (16:29:47.3388, −48°15′52.3963″).

To investigate the kinematics of the molecular gas in G335.79+0.17, the emission from CH_3CN and CH_3CCH was used. These molecular transitions provide a means to analyze the gas distribution and serve as a basis for understanding the internal dynamics and evolutionary processes within the P1 and P2 cores. Figure

3 presents the moment 0, 1 and 2 maps of the K = 3 rotational transitions of CH_3CN (J = 15 → 14; upper panel) and CH_3CCH (17 → 16; lower panel) toward cores P1 and P2.

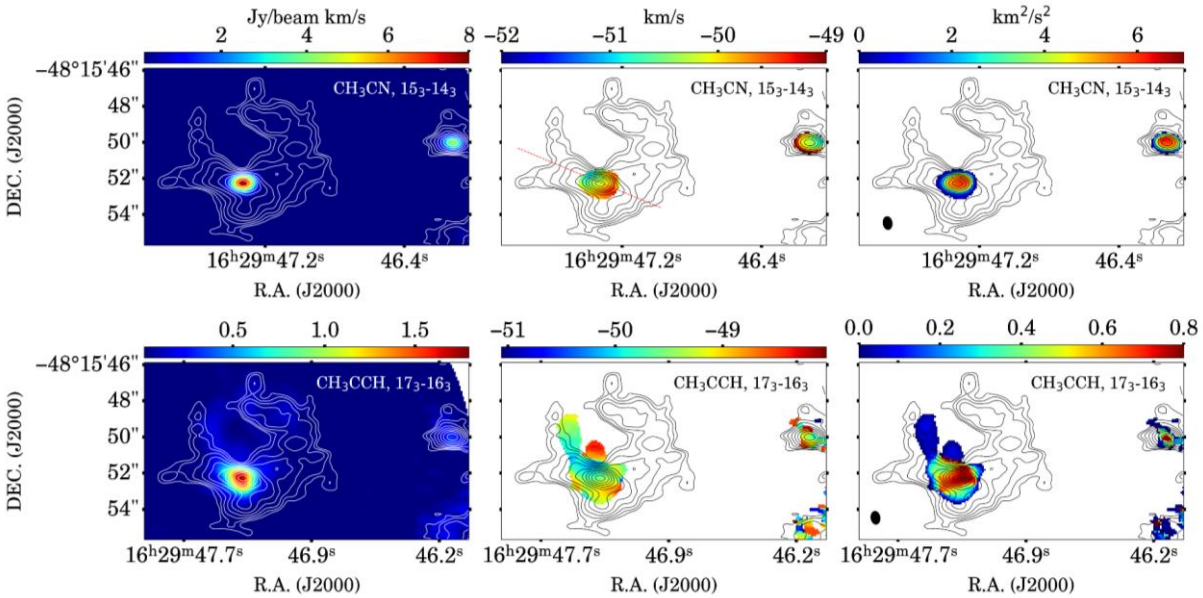

Fig. 3. Moment 0 (left column), moment 1 (middle column), and moment 2 (right column) maps of the CH_3CN ($15_3 \rightarrow 14_3$, top panels) and CH_3CCH ($17_3 \rightarrow 16_3$, bottom panels) transitions. Superimposed are contours of the continuum emission. Contours are plotted at 1σ, 5σ, 20σ, 100σ, and 600σ, where σ = 0.005 Jy beam^{-1}. The black ellipse shown in the bottom left corner indicates the synthesized beam size.

In the moment 0 maps of CH_3CN the peak intensity is ~8 Jy beam^{-1} km s^{-1} in core P1 and ~3 Jy beam^{-1} km s^{-1} in core P2. In the moment 1 maps, core P1 exhibits a velocity gradient of ~3 km s^{-1} oriented from northeast to southwest across all three components. The gradient direction is highlighted by the red dashed line in Figure 3, corresponding to a position angle of 68°. A similar dual-core structure has been reported by [27], and comparable gradients have been observed in G333.6–0.2 [28] and G301.1364–00.2249 A [29]. Core P2 also shows a velocity gradient of ~3 km s^{-1}, oriented from northwest to southeast. These gradients provide clear evidence of rotational motions in the molecular gas, and the gradients in cores P1 and P2 display a symmetric configuration. In the moment 2 maps, the velocity dispersion in the central regions of both cores reaches ~6 km^2 s^{-2}. Such high dispersions are typical of hot molecular cores, suggesting that the gas is embedded in a dense medium with substantial turbulence.

In the moment 0 maps of CH_3CCH, the peak intensity in core P1 reaches ~1.5 Jy beam^{-1} km s^{-1}, whereas in core P2 the emission is weaker (~0.7 Jy beam^{-1} km s^{-1}). The velocity gradients observed in the moment 1 maps for both cores are consistent with those traced by methyl cyanide (CH_3CN), confirming the reliability of the inferred kinematic structures. However, in the northern region of core P1, the methylacetylene emission reveals additional localized velocity features. In particular, elongated streamer-like structures are identified, exhibiting a clear south–north velocity gradient [30]. The velocity dispersion (moment 2) is enhanced in the central region of core P1, reaching values up to 0.8 km^2 s^{-2}, indicative of turbulence characteristic of hot molecular cores [31]. These streamer-like features, visible in the moment 1 map, are not associated with significant velocity dispersion in moment 2, suggesting relatively ordered motions rather than turbulence-dominated kinematics.

The emission morphology of CH_3CN and CH_3CCH is similar, with the integrated intensity peaks coinciding with the dust continuum peaks toward cores P1 and P2, indicating dense gas and confirming the presence of hot molecular cores. The inferred rotation of the molecular gas is roughly perpendicular to the CO outflow axis, traced by ^{13}CO (6–5) and ^{12}CO (6–5) [32]. The detected maser emission toward both cores further indicates compact, dense, and dynamically active regions associated with massive star formation.

The rotational temperature and total column density of the lines were derived using MAdrid Data CUBe Analysis (MADCUBA) assuming local thermodynamic equilibrium (LTE) [33]. The physical parameters are

calculated based on the population diagram method, where the relationship between the upper-level column density and the excitation energy is expressed by the following rotation diagram equation:

$$log\left(\frac{N_u^{thin}}{g_u}\right) = -\left(\frac{log\ \mathrm{e}}{\mathrm{T}_{rot}}\right)\left(\frac{\mathrm{E}_u}{k_\mathrm{B}}\right) + log\left(\frac{N_{total}}{Q\ (\mathrm{T}_{rot})}\right) \quad (1)$$

where N_u^{thin} represents the column density in the upper level, g_u is the statistical weight, T_{rot} is the rotational temperature, E_u is the upper-level energy, k_B is the Boltzmann constant, N_{total} is the total column density, and $Q(T_{rot})$ is the partition function.

Figure 4 shows the population diagrams derived from this linear relationship: the left panels correspond to the CH_3CN (J = 15 → 14) transitions, the middle panels to $CH_3{}^{13}CN$ (J = 15 → 14) and the right panels to CH_3CCH (J = 17 → 16). The derived rotational temperatures and column densities for cores P1 and P2 are summarized in Table 2. The uncertainty on T_{rot} was obtained from the standard error of the linear fit to the rotation diagram as calculated by MADCUBA. Table 2 shows that the highest rotational temperature is obtained from methyl cyanide (553 ± 72.2 K), while significantly lower values are derived from CH_3CCH (117.6 ± 17.4 K) and $CH_3{}^{13}CN$ (229.2 ± 67.6 K).

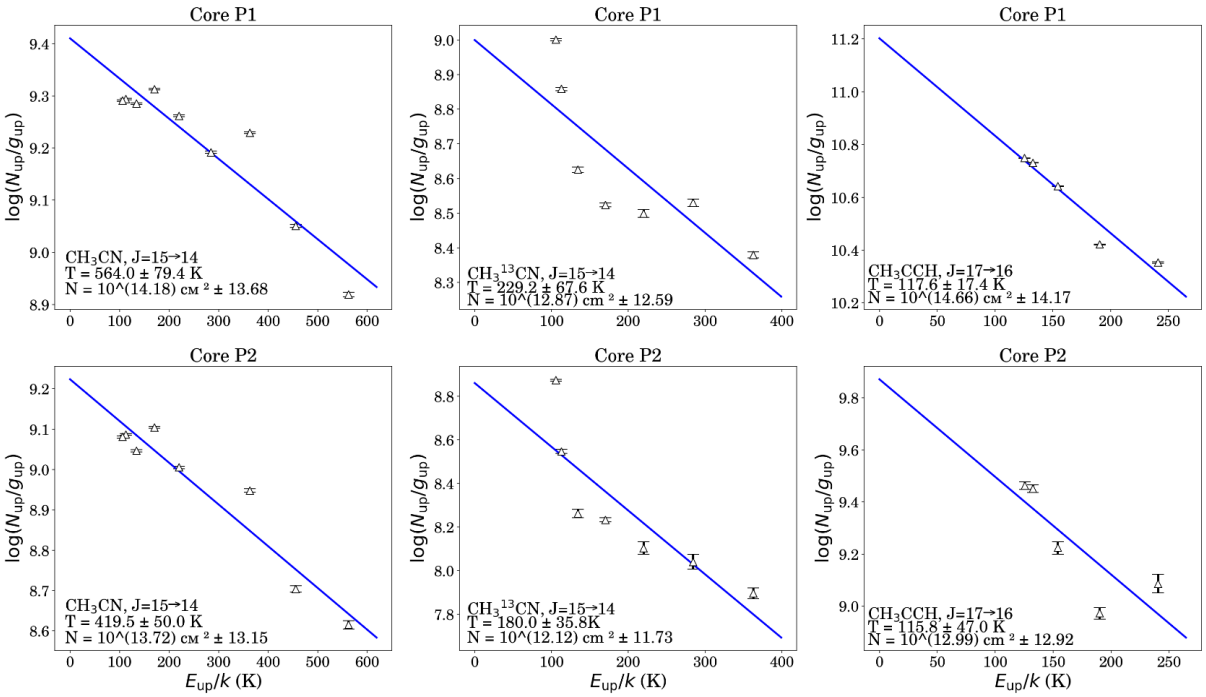

Fig.4. Population diagrams of CH_3CN (J = 15 → 14; left panels), $CH_3{}^{13}CN$ (J = 15 → 14; middle panels), and CH_3CCH (J = 17 → 16; right panels) for cores P1 (top row) and P2 (bottom row). The blue solid lines represent the best linear fits to the data points.

Table 2. Rotational temperatures and total column densities derived from the population diagram analysis for CH_3CN, $CH_3{}^{13}CN$ and CH_3CCH toward cores P1 and P2.

Species	T_{rot} (K)		N (cm^{-2})	
	Core P1	Core P2	Core P1	Core P2
CH_3CN	553 ± 72.2	419.5 ± 50	1.51×10^{14}	5.24×10^{13}
$CH_3{}^{13}CN$	229.2 ± 67.6	172.9 ± 35.8	6.91×10^{12}	2.57×10^{12}
CH_3CCH	117.6 ± 17.4	115.8 ± 47	4.57×10^{14}	5.24×10^{13}

The discrepancies among these temperatures indicate that the molecules trace distinct gas layers within the hot core. CH_3CN desorbs from dust grains at radii closer to the protostar-where the gas is warmer-naturally

accounting for the higher temperature measured from this species. In contrast, CH_3CCH desorbs at larger radii, corresponding to cooler regions [34]. The integrated intensity maps further support this interpretation, showing that CH_3CN emission is more compact, while CH_3CCH emission is more extended, particularly toward the northeast. Taken together, the results demonstrate that core P1 is substantially hotter and denser than core P2.

4. Conclusion

The HMYSO G335.79+0.17 was studied using ALMA Band 7 observations. The emission of molecular lines coincides with the dust continuum peaks, revealing two distinct hot cores: P1 and P2.

Rotational diagram analysis of CH_3CN and CH_3CCH yields temperatures of 553 ± 72, 229 ± 68 and 118 ± 17 K for P1, with corresponding column densities of 1.51×10^{14}, 6.91×10^{12} and 4.57×10^{14} cm^{-2}. For P2, the temperatures are 420 ± 50, 173 ± 36 and 116 ± 47 K, with column densities of 5.24×10^{13}, 2.57×10^{12} and 5.24×10^{13} cm^{-2}. These results indicate that core P1 is significantly hotter and denser than P2, exhibiting stronger emission and a more pronounced velocity structure, highlighting its dominant dynamical activity.

Velocity gradients were detected in both cores, oriented northeast–southwest in P1 and northwest–southeast in P2, with opposite redshifted directions, providing strong evidence of rotational motions within both cores. The turbulence and central maser emission confirm that the hot cores are dynamically active sites of massive star formation, whereas the nearby streamer-like structures exhibit markedly lower turbulence, indicative of more ordered kinematics.

These results directly address the goal of this study: the observed rotational motions appear to play a critical role in regulating gas accretion and driving the star formation process in G335.79+0.17, thereby clarifying the evolutionary stage of the embedded high-mass young stellar object.

Conflict of interest statement

The authors declare that they have no conflict of interest in relation to this research, whether financial, personal, authorship or otherwise, that could affect the research and its results presented in this paper.

CRediT author statement

Abdirakhman A.A., Omar A.Zh.: Conceptualization, Investigation, Formal analysis, Writing Original draft**; Alimgazinova N.Sh.:** Methodology, Writing - Review & Editing; **Tuiakbayeva D.R., Baitursyn D.Y.:** Data Curation, Visualization.
The final manuscript was read and approved by all authors.

Acknowledgements

This research was funded by the Science Committee of the Ministry of Science and Higher Education of the Republic of Kazakhstan (Grant No. AP26102915).

This paper makes use of the following ALMA archival data: ADS/JAO.ALMA#2021.1.00720. S. ALMA is a partnership of ESO (representing its member states), NSF (USA), and NINS (Japan), together with NRC (Canada), MOST and ASIAA (Taiwan), and KASI (Republic of Korea), in cooperation with the Republic of Chile.

The Joint ALMA Observatory is operated by ESO, AUI/NRAO, and NAOJ.

References

1 Tan J. C., Beltrán M. T., Caselli P., Fontani F., Krumholz M. R., McKee C. F., & Stolte A. (2014) *Massive star formation* [arXiv preprint]. arXiv. https://doi.org/10.48550/arXiv.1402.0919

2 Berdikhan D., Esimbek J., Henkel C., Zhou J., Tang X., Liu T., Wu G., Li D., He Y., Komesh T., Tursun K., Zhou D., Imanaly E., & Jandaolet Q. (2024) Ammonia observations of Planck cold cores. *Astronomy & Astrophysics*, 684, A144. https://doi.org/10.1051/0004-6361/202348381

3 Sailanbek S., Esimbek J., Henkel C., Sobolev A. M., Ladeyschikov D. A., Berdikhan D., Wu G., Zhou J., Tang X., He Y., Li D., Tursun K., Zhou D., Ma Y., Komesh T., Ibraimov M., & Adilzhan K. (2025) Ammonia survey of the BGPS sources with the Nanshan 26-m telescope. *Monthly Notices of the Royal Astronomical Society*, 539, 2987–3012. https://doi.org/10.1093/mnras/staf564

4 Fukui Y., Habe A., Inoue T., Enokiya R., & Tachihara K. (2021) Cloud–cloud collisions and triggered star formation. *Publications of the Astronomical Society of Japan, 73* (Supplement_1), S1–S34. https://doi.org/10.1093/pasj/psaa103

5 Berdikhan D., Esimbek J., Henkel C., Xu Y., Zhou J., Liu D. J., Abdikamalov E., Ma Y., Komesh T., He Y., Zhang W., Tang X., Wu G., Li D., Zhou D., Tursun K., Shen H., Imanaly E., Jandaolet Q., & Tuiakbayeva D. (2025)

Cloud-cloud collision and star formation in G013.313+0.193. *Astronomy & Astrophysics*, 699, A137. https://doi.org/10.1051/0004-6361/202453285

6 Li D., Henkel C., Kraus A., Tang X., Baan W., Esimbek J., Wang K., Wu G., Liu T., Sobolev A. M., Zhou J., He Y., & Komesh T. (2025) Evidence for Core–Core Collision in Barnard 68. *The Astrophysical Journal*. 985, 230. https://doi.org/10.3847/1538-4357/add326

7 Ussipov N., Akhmetali A., Zaidyn M., Akniyazova A., Sakan A., Kalambay M., & Shukirgaliyev B. (2024) Fractal dimension of star clusters. *Eurasian Physical Technical Journal, 21*(3), 108–116. https://doi.org/10.31489/2024No3/108-116

8 Ma Y., Zhou J., Esimbek J., Baan W., Li D., Tang X., He Y., Ji W., Zhou D., Wu G., Tursun K., & Komesh T. (2023) Gravitational collapse and accretion flows in the hub filament system G323.46-0.08. *Astronomy & Astrophysics*, 676, A15. https://doi.org/10.1051/0004-6361/202346248

9 He Y. X., Liu H. L., Tang X. D., Qin S. L., Zhou J. J., Esimbek J., Pan S. R., Li D. L., Zhao M. K., Ji W. G., & Komesh T. (2023) Investigating the globally collapsing hub–filament cloud G326.611+0.811. *The Astrophysical Journal*, 957, 61. https://doi.org/10.3847/1538-4357/acf766

10 Zhang W., Zhou J., Esimbek J., Baan W., He Y., Tang X., Li D., Ji W., Wu G., Ma Y., Li J., Zhou D., Tursun K., & Komesh T. (2024) Kinematics and star formation of hub-filament systems in W49A. *Astronomy & Astrophysics*, 688, A99. https://doi.org/10.1051/0004-6361/202348580

11 Meng D., Esimbek J., Henkel C., Zhou J., Wu G., Tang X., Li D., He Y., Komesh T., Ma Y., Tursun K., Zhou D., Baan W., Sobolev A. M., Sailanbek S., & Jandaolet Q. (2025) A case investigation of an end-dominated collapse and hub-filament system, G53. *Astronomy & Astrophysics*, 701, A155. https://doi.org/10.1051/0004-6361/202453390

12 Li D., Esimbek J., Zhou J., Baan W., Wu G., Tang X., Ji W., Yuan Y., He Y., & Komesh T. (2016) KOSMA ^{12}CO (2–1) and (3–2) observations toward Infrared Dark Clouds. *Astrophysics and Space Science*, 361, 220. https://doi.org/10.1007/s10509-016-2807-z

13 Shen H., Esimbek J., Henkel C., Xu Y., Zhou J., Li D., He Y., Tang X., Wu G., Komes T., Tursun K., Zhou D., Imanaly E., & Berdikhan D. (2024) Extended CO (1–0) survey and ammonia measurements towards two bubble regions in W5: Feedback on molecular gas and clumps. *Astronomy & Astrophysics*, 689, A140. https://doi.org/10.1051/0004-6361/202347972

14 Shen H., Esimbek J., Henkel C., Li D., Zhou J., He Y., Tang X., Wu G., Komes T., Tursun K., Zhou D., Ma Y., Sailanbek S., & Berdikhan D. (2025) Triggered and dispersed under feedback of super HII region W4. *Astronomy & Astrophysics*, 693, A21. https://doi.org/10.1051/0004-6361/202450914

15 Herbst E., & Van Dishoeck,E. F. (2009).*Complex organic interstellar molecules. Annual Review of Astronomy and Astrophysics, 47*(1), 427–480. https://doi.org/10.1146/annurev-astro-082708-101654

16 Kalenskii S. V., Promislov V. G., Alakoz A., Winnberg A. V., & Johansson L. E. (2000) Probing the properties of methyl cyanide sources. *Astronomy and Astrophysics*, 354, 1036-1040. https://ui.adsabs.harvard.edu/abs/2000A&A...354.1036K

17 Komesh T., Esimbek J., Baan W., Zhou J., Li D., Wu G., He Y., Sailanbek S., Tang X., & Manapbayeva A. (2019) *H_2CO and H110α observations toward the Aquila Molecular Cloud. The Astrophysical Journal, 874*(2), 172. https://doi.org/10.3847/1538-4357/ab0ae3

18 Komesh T., Baan W., Esimbek J., Zhou J., Li D., Wu G., He Y., Rosli Z., & Ibraimov M. (2020) Studies of the distinct regions due to CO selective dissociation in the Aquila molecular cloud. *Astronomy & Astrophysics*, 644, A46. https://doi.org/10.1051/0004-6361/202038632

19 Mahmut U., Esimbek J., Baan W., Tang X., Zhou J., Li D., Yuxin H., Tursun K., Li J., Komesh T., & Sailanbek S. (2024) Formaldehyde observations of the Perseus Molecular Cloud. *Monthly Notices of the Royal Astronomical Society*, 528, 577–595. https://doi.org/10.1093/mnras/stad3959

20 Bu J., Esimbek J., Zhou J., Komesh T., Tang X., Li D., He Y., Tursun K., Zhou D., Imanaly E., & Sailanbek S. (2024) Calculating the Excitation Temperature for H_2CO Absorption Lines in Molecular Clouds. *Research in Astronomy and Astrophysics*, 24, 075022. https://doi.org/10.1088/1674-4527/ad5b36

21 Imanaly E., Esimbek J., Baan W., Wu G., Zhou J., Li D., Tang X., He Y., Komesh T., Zhou D., Tursun K., Ma Y., Berdikhan D., Sobolev A. M., & Jandaolet Q. (2025) Formaldehyde in the Cygnus-X region. *Monthly Notices of the Royal Astronomical Society*, 542, 2074–2086. https://doi.org/10.1093/mnras/staf1346

22 Smits D. P. (2003) *Monitoring of 6-cm excited OH masers—II. Monthly Notices of the Royal Astronomical Society*, 339(1), 1–11. https://doi.org/10.1046/j.1365-8711.2003.06096.x

23 Sakai T., Shiomura N., Sanhueza P., Furuya K., Olguin F. A., Tatematsu K. I., Aikawa Y., Taniguchi K., Chen H. R. V., Morii K., Nakamura F., Li S., Lu X., Zhang Q., Hirota T., Ishihara K., Ke H., Sakai N., & Yamamoto S. (2025) Digging Into the Interior of Hot Cores with ALMA (DIHCA). V. Deuterium Fractionation of Methanol. *The Astrophysical Journal*, 983, 37. https://doi.org/10.3847/1538-4357/adba5a

24 He Y. X., Zhou J. J., Esimbek J., Ji W. G., Wu G., Tang X. D., Yuan Y., & Baan W. A. (2015) Infall motions in massive star-forming regions: results from years 1 and 2 of the MALT90 survey. *Monthly Notices of the Royal Astronomical Society*, 450, 1926–1936. https://doi.org/10.1093/mnras/stv732

25 Abdullayev Z., Komesh T., Grossan B., Abdikamalov E., Maksut Z., Krugov M., Myrzakul S., & Tuiakbayeva D. (2025) Early-time optical spectral shape measurements of GRB 200925B. Revista Mexicana de Astronomía y Astrofísica (Serie de Conferencias), 59, 109–113. https://doi.org/10.22201/ia.14052059p.2025.59.20

26 McMullin J. P., Waters B. S. D. Y. W. G. K., Schiebel D., Young W., & Golap K. (2007). CASA architecture and applications. *In Astronomical data analysis software and systems XVI* (Vol. 376, p. 127). https://adsabs.harvard.edu/full/2007ASPC..376..127M

27 Komesh T., Omar A., Garay G., Assembay Z., Alimgazinova N., Zhumabay N., & Kyzgarina M. (2021) *ALMA observations of the environments of G333.0162+00.7615*. In T. Wong & W.-T. Kim (Eds.), *Proceedings of the International Astronomical Union* (Vol. 17, pp. 35–38). Cambridge University Press. https://doi.org/10.1017/S1743921323000121

28 Omar A., Abdirakhman A., Alimgazinova N., Kyzgarina M., Naurzbayeva A., Islyam Z., Turekhanova K., Demessinova A., & Manapbayeva A. (2025) ALMA Observations of G333.6-0.2: Molecular and Ionized Gas Environment. Galaxies. 13, 73. https://doi.org/10.3390/galaxies13040073

29 Assembay Z., Komesh T., Garay G., Omar A., Esimbek J., Alimgazinova N., Kyzgarina M., & Murat S. (2022) *ALMA observations of the environments of G301.1364-00.2249 A.* In T. Hirota, H. Imai, K. Menten, & Y. Pihlström (Eds.), *Proceedings of the International Astronomical Union* (Vol. 18, S380, pp. 204–206). Cambridge University Press. https://doi.org/10.1017/S1743921323002624

30 Hales A. S., Gupta A., Ruíz-Rodríguez D., Williams J. P., Pérez S., Cieza L., González-Ruilova C., Pineda J. E., Santamaría-Miranda A., Tobin J., Weber P., Zhu Z., & Zurlo A. (2024) Discovery of an accretion streamer and a slow wide-angle outflow around FU Orionis. *The Astrophysical Journal*, 966, 96. https://doi.org/10.3847/1538-4357/ad31a1

31 Komesh T., Garay G., Henkel C., Omar A., Estalella R., Assembay Z., Li D., Guzmán A., Esimbek J., Huang J., He Y., Alimgazinova N., Kyzgarina M., Bekdaulet S., Zhumabay N., & Manapbayeva A. (2024) Infall motions in the hot core associated with the hypercompact H II region G345.0061+01.794 B. *The Astrophysical Journal*, 967, 15. https://doi.org/10.3847/1538-4357/ad3e7b

32 Hoang T. D., Lee M. Y., Wyrowski F., Karska A., Navarete F., & Menten K. M. (2025) ATLASGAL-selected high-mass clumps in the inner Galaxy: XI. Morphology and kinematics of warm inner envelopes. *Astronomy & Astrophysics, 695,* A24. https://doi.org/10.1051/0004-6361/202452371

33 Martín S., Martín-Pintado J., Blanco-Sánchez C., Rivilla V. M., Rodríguez-Franco A., & Rico-Villas F. (2019) Spectral line identification and modelling (SLIM) in the MAdrid Data CUBe analysis (MADCUBA) package: Interactive software for data cube analysis. *Astronomy & Astrophysics, 631,* A159. https://doi.org/10.1051/0004-6361/201936144

34 Andron I., Gratier P., Majumdar L., Vidal T. H. G., Coutens A., Loison J.-C., & Wakelam V. (2018) Methyl cyanide (CH_3CN) and propyne (CH_3CCH) in the low-mass protostar IRAS 16293–2422. *Monthly Notices of the Royal Astronomical Society*, 481(4), 5651–5659. https://doi.org/10.1093/mnras/sty2680

AUTHORS' INFORMATION

Abdirakhman, Aidana A. — Master's student, Faculty of Physics and Technology, Al-Farabi Kazakh National University, Almaty, Kazakhstan; Scopus Author ID: 60077369400; https://orcid.org/0009-0002-0532-964; armiyaqyzyaidana@gmail.com.

Omar, Aruzhan Zh. — PhD, Senior lecturer, Faculty of Physics and Technology, Al Farabi Kazakh National University, Almaty, Kazakhstan; Scopus Author ID: 58420497300; https://orcid.org/0000-0002-5604-3742; omaruzhan@gmail.com.

Alimgazinova, Nazgul Zh. — Candidate of physical and mathematical sciences, Associate Professor, Faculty of Physics and Technology, al Farabi Kazakh National University, Almaty, Kazakhstan; Scopus Author ID: 35298349000; https://orcid.org/0000-0002-4596-1855; Nazgul.Alimgazinova@kaznu.kz.

Tuiakbayeva, Duriya R. — Master (Sci.), Sh. Ualikhanov Kokshetau University, Kokshetau, Kazakhstan; Scopus Author ID: 58829147000; https://orcid.org/0009-0003-8572-1850

Baitursyn, Darkhan Y. — Master (Eng.), Astana Motors Manufacturing Kazakhstan, Almaty, Kazakhstan; https://orcid.org/0009-0007-7398-4222; baitursyndarhan@gmail.com.